ATH5305
/AN

Galley Proofs ± 11p

Atherosclerosis VOL (1994) PP–PP

Evaluation of computerized edge tracking for quantifying intima-media thickness of the common carotid artery from B-mode ultrasound image

Robert H. Selzer*[a], Howard N. Hodis[b], Helenann Kwong-Fu[a], Wendy J. Mack[b], Paul L. Lee[a], Chao-ran Liu[b], Ci-hua Liu[b]

[a]*M/S 168-514, Jet Propulsion Laboratory, California Institute of Technology, 4800 Oak Grove Drive, Pasadena, CA 91109, USA*
[b]*Atherosclerosis Research Institute, University of Southern California School of Medicine, Los Angeles, CA, USA*

Received 23 September 1993; revision received 3 May 1994; accepted 18 May 1994

Abstract

A new method to measure carotid intima-media thickness (IMT) from B-mode ultrasound images was developed that utilizes automatic tracking of the lumen-intima and media-adventitia echoes. Phantom studies and human replicate studies under typical clinical protocols for common carotid IMT measurement were carried out to assist in evaluation of the method. A lucite step wedge phantom was used to show that incorporation of sub-pixel interpolation to locate echo boundaries allowed detection of changes in the echo separation that were 5–10 times smaller than the axial resolution of the ultrasound transducer. For average IMT measured in the distal common carotid artery (CCA) wall in 24 subjects scanned twice within 60 days, mean absolute difference was 0.036 mm with a standard deviation of 0.045 mm. Replicate scans obtained 1 week apart of eight subjects by three sonographers showed the inter-sonographer variability was 5.4%. In another study of 12 subjects scanned every 4 months for 48 months, the root mean square deviation of the IMT measurements from a linear regression line was 0.030 mm. These data indicate that the method is equally precise over short intervals (60 days) and over long intervals (48 months). The new automated computerized edge tracking method presented in this paper represents an advance for image analysis of B-mode ultrasound images of common carotid IMT with measurement variability substantially reduced (2 to 4 times) compared with currently available manual methods.

Keywords: Carotid arteries; Ultrasound; Atherosclerosis

* Corresponding author.

SSDI 0021-9150(94)05305-3

1. Introduction

Dear Author,
Please return corrections as soon as possible
by fax or courier. Originals by Express Mail

Brian O'Halloran

UNCORRECTED PROOFS

Since the lumen-intima and media-adventitia echoes in carotid ultrasound images were identified by Pignoli et al. in 1986 [1], B-mode ultrasonography has been used for non-invasive quantitative measurement of intima-media thickness (IMT) as a primary indicator of atherosclerotic disease [1–4] in a number of epidemiologic studies [5–11]. These studies have relied on human visual judgement to manually identify echo coordinates with a computer pointing device, either at discrete points [9,10] or along a continuous trace of the border [2,3,7,8]. The accuracy and precision of IMT measurements determined by manual pointing methods are limited by human variability in operation of the pointing devices and by the resolution of the displayed ultrasound image. It is our belief that automated IMT measurement with a computerized edge detection algorithm greatly improves the accuracy and precision of such measurements for two major reasons: (1) the component of variability associated with manual cursor placement is eliminated and (2) the automated edge tracking using sub-pixel interpolation determines edge boundaries at a resolution greater than monitor line resolution.

To test this new automated method, we used a lucite phantom to determine the minimum detectable change in separation of two acoustic reflectors. This study was carried out partially to disprove the common belief that detection of change is limited by the axial resolution of the ultrasound transducer. With this phantom, the distance between two acoustic interfaces could be varied by increments as small as 0.025 mm. Additionally, we performed a series of studies with single and multiple sonographers and analyzed replicate scans of the distal CCA far wall IMT to determine measurement variability over a short-term period of 60 days and over a long-term period of 48 months.

2. Methods

2.1. Ultrasound imaging systems

All images in this study were acquired in the Ultrasound Laboratory of the Atherosclerosis Research Institute of the University of Southern California School of Medicine. Except those for subjects in the Monitored Atherosclerosis Regression Study (MARS), images were acquired with a Toshiba SSH 140A Ultrasound System, operating in B-mode with a 7.5 MHz transducer and recorded on 0.5 inch video tape with a Panasonic 7355 S-VHS video cassette recorder (VCR). Subjects in the MARS study were scanned with a Diasonics CV400 ultrasound system using a 7.5 MHz probe and images recorded on 0.75 inch video tape with a Sony VO 5850 VCR. The images from the MARS subjects were copied to 0.5 inch SVHS video tape prior to computer analysis. In all studies, an ECG signal was superimposed on the ultrasound image.

2.2. Image processing system

Ultrasound images were analyzed at end diastole with a Northgate 386/33 computer system equipped with a Data Translation DT 2862 digitizing and image processing board. The Data Translation board converts a video image into a 512 by 480 digital array with 256 grey levels per picture element. Playback of the ultrasound tapes was carried out with a Panasonic 7355 S-VHS VCR whose output was fed to the Data Translation board. This VCR contains a digital memory that allows the computer to digitize a full 480 line video frame with the VCR in still mode. VCRs without frame memory display only half-frame fields (240 lines) in still mode. Since accurate frame selection for IMT measurement requires the use of VCR still mode display, the frame memory is essential to obtain full image resolution in the digitized image. Images are digitized to full frame resolution when the VCR is in normal play mode, but frame selection is very difficult with the tape moving at normal playback speed. Although the Panasonic 7355 contains a digital frame memory, the digital data are not accessible to the computer. The only VCR output is an analog signal derived from the frame buffer and, as a result, a digitizing board is required in the computer.

The process of digitizing the video ultrasound image, tracking the lumen-intima and media-adventitia echoes and computing IMT is accomplished with a PC computer program named PROSOUND (copyright, University of Southern California), [redacted]. Details of the algorithms used by PROSOUND are described below.

2.3. Edge tracking method

The lumen-intima and media-adventitia echoes are located with a three-step computer method as follows: (1) an approximate echo boundary is identified with a mouse; (2) the approximate boundary is used to guide the computer edge finding algorithm to locate an initial or conditional set of edges; (3) the initial computer edges are tested for 'edge strength' and false or weak edges are eliminated. A further description of each of these steps is given below.

Edge tracking step 1: determine an approximate echo boundary. This is accomplished by pointing to the leading edge of the echo at a few points with a mouse. The computer then fits a smooth continuous curve to these points.

Edge tracking step 2: determine 'conditional' edge coordinates. The computer algorithm searches for edges in a direction perpendicular to the approximate boundary. At each point of the approximate boundary, 13 pixels in the image are examined that lie along a line perpendicular to this boundary. Half of the examined points are selected from one side of the approximate boundary and half from the other. Since the approximate boundary is selected to coincide visually with the leading edge of the echo, coordinates of the 'true' edges usually fall within plus or minus 3–4 pixels of the approximate boundary. The computer-determined echo boundary is determined as the point within the 13 pixel sequence at which the rate of intensity change (or gradient) of the pixels is a maximum. Fig. 1 shows an example of the pixel intensity values and the resulting computed gradient for one boundary point.

The rate of change of intensity at a particular pixel in the sequence is computed as the derivative of a second degree polynomial fit to the five pixels centered on the pixel in question. This process is repeated for each of the pixels, beginning with the third and ending with the eleventh. The integer location in the image of the pixel with the largest gradient was initially taken as the echo boundary, but, as discussed below, we determined that the maximum gradient of the pixel sequence can occur between pixels and that edges determined to 'sub-pixel' resolution are more accurate than edges determined to integer pixel resolution. To understand the concept of sub-pixel edge detection resolution, consider the situation where two identical maximum gradient values occur for adjacent pixels. In this case, the maximum gradient for the sequence is selected as mid-way between the two pixels.

To find the sub-pixel maximum gradient location, the nine gradient values corresponding to integer pixel locations as described above are searched to find the largest value and a parabola is fitted to the three gradient values centered on the largest value. The coordinate of the parabola maximum is taken as the sub-pixel edge location. As demonstrated below, calculation of boundaries at sub-pixel resolution improves accuracy of edge detection.

The coordinates of the edges found in step 2 are labeled as conditional edges and are converted to true edges or discarded, according to the method described in step 3.

Edge tracking step 3: eliminate weak edges. After conditional edges are determined for all points, the gradient value for each edge is compared with the maximum gradient value of all conditional edges. Edge points with gradient values less than 20% of the maximum value are deleted. The remaining edges are deemed acceptable. This procedure minimizes identification of spurious edge points due to image noise.

For a range of carotid images obtained with the Toshiba ultrasound scanner, spurious edges tended to be accepted when the threshold was ~~higher~~ lower than 20% and valid low intensity edges tended to be rejected when the threshold was ~~lower~~ higher. The 20% threshold also worked well with the images from the Biodynamics and Diasonics scanners.

2.4. IMT calculation

After the edge tracking process has been applied to the lumen-intima and the media-adventitia echoes, IMT is computed for all acceptable edge point pairs as the mean separation between the two edges. As part of the process of identifying acceptable edge point pairs, gaps in the lumen-intima boundary due to deleted edges are temporarily filled by linear interpolation from the nearest acceptable edges. Then, for each acceptable media-adventitia edge, a line is drawn that is locally perpendicular to the media-adventitia edges and intersects the lumen-intima boundary. If the lumen-

intima edge closest to this line was originally an acceptable edge (i.e. not an interpolated edge), it is paired with the media-adventitia edge and the IMT distance calculated. If the nearest lumen-intima edge is an interpolated edge, the media-adventitia edge under consideration is assumed not to have a matching edge and the process is repeated for the next media-adventitia edge. Average IMT is computed as the mean of the acceptable edge-point pairs. On average, acceptable matching edge points were found for 77.5% of the 1 cm wall images from 26 subjects discussed below. A 1 cm length of the carotid wall is represented by 84 pixels in an image from the Toshiba scanner.

2.5. Step wedge phantom study methods

To estimate the minimum change in separation of two acoustic interfaces that could be detected using the automated edge tracking algorithm, a step wedge phantom was constructed. The phantom was fabricated from two 40 mm × 30 mm × 15 mm lucite blocks. Six steps each 5 mm wide were cut into the surface of one block to depths varying from 0.27 to 1.53 mm. The depth of each step was measured to an accuracy of 0.010 mm with a Panasonic Acurite optical microscope comparator. The blocks were placed together as shown in Fig. 2, submerged in water, and scanned with the Toshiba system with the probe mechanically clamped to a wooden stand. Metal shims 0.028 mm thick were then inserted between the blocks to increase the separation of all steps by the width of the shims and the resulting phantom was re-scanned. This process was repeated with additional metal shims until images of water-filled gaps in the lucite had been acquired ranging from 0.27 to 1.76 mm in 0.028 mm steps. Images acquired with the Toshiba SSH 140 Ultrasound Scanner were converted to digitized images with 512 pixels per row and 480 rows. The separation represented by each pixel was 0.119 mm in the horizontal direction and 0.096 mm in the vertical direction. The automated edge tracking program was used to locate the top and bottom edges of each gap along a distance of approximately 3 mm (25 pixels) and to compute the average size of each gap.

2.6. Human replication study methods, short-term variability

Twenty-four subjects participating in a study of slow-release niacin received replicate carotid ultrasound scans of the far wall of the distal right CCA. The interval between the first and second scan was less than 60 days. Subjects were 58% male (n = 14) with an average age of 52.6 years (range 22–74) at the first ultrasound examination. The majority (87%) of these subjects were non-smokers, and they had an average (S.D.) systolic blood pressure of 115.7 (13.5) mmHg and diastolic blood pressure of 75.0 (8.3) mmHg. Average (S.D.) lipid and lipoprotein levels at baseline were: total cholesterol, 261.0 (23.9) mg/dl; LDL cholesterol, 186.9 (17.8) mg/dl; HDL cholesterol, 43.1 (10.1) mg/dl; triglycerides, 138.7 (65.5) mg/dl.

To determine intersonographer variability, eight subjects were scanned three times each by three sonographers. Two scans were obtained during the same examination, with the subject sitting up and then being repositioned between scans. The third examination was 1 week after the first.

2.7. Human replication study methods, long-term variability

In a study of 12 subjects from the MARS trial, IMT measurements were made from the distal CCA far wall from ultrasound examinations acquired at 3–4 month intervals for 48 months [12]. Ten subjects were male and two female, the average age of the 12 subjects being 59.5 years at the start of the first ultrasound examination. Four of the subjects had never smoked, seven were ex-smokers and one currently smoked. Average (S.D.) lipid and lipoprotein levels at baseline were: total cholesterol, 233.0 (20.2) mg/dl; LDL cholesterol, 153.9 (21.2) mg/dl; HDL cholesterol, 48.3 (21.7) mg/dl; triglycerides, 154.2 (58.8) mg/dl.

For each subject, a linear regression line was fitted to the IMT measurements acquired over 48 months and a calculation was made of the mean absolute difference and root mean square (RMS) deviation of IMT from the regression line. Fig. 3 shows IMT values acquired over 4 years for two of the subjects. The resulting mean absolute difference (MAD) and RMS error values, averaged over the 12 subjects, are conservative estimates of precision since the true error is overestimated if the assumption of linear IMT change over time is not true.

Note to editor
* we haven't defined S.D. before this point in the paper.

2.8. Protocol for acquisition and processing of human scans

For both the short- and the long-term studies, an antero-lateral longitudinal view of the far wall of the right CCA was obtained with the head approximately 45° in the contra-lateral direction. The lumen-intima and media-adventitia echoes are optimally visualized when the scan lines are perpendicular to the wall. With the probe between 30° and 45° to the horizontal, it was positioned to maximize the brightness of the lumen-intima echo and to minimize gaps in the echo. When the ultrasound beam is approximately normal to the wall, the reflected signal from the lumen-intima interface is maximized and produces the brightest signal. Similarly, the lumen-intima echo has the fewest gaps when the plane of the image is parallel to the vessel axis.

The proximal portion of the bulb was included in the image for reference purposes. One sonographer carried out all ultrasound scans for the short-term and long-term studies. All scans were carried out using the lowest power and signal gain consistent with visualization of the wall echoes.

Video tapes were analyzed by an operator who selected one end diastolic frame from a 5–10 s recording using maximum lumen-intima continuity and maximum lumen-intima echo brightness as selection criteria. Average IMT was computed over a 1 cm length of the CCA far wall ending approximately 0.5 cm proximal to the transition between the common carotid and bulb regions. The dividing point between the regions was identifiable in most cases by a relatively abrupt change in the angle of the far wall at the beginning of the bulb as shown in Fig. 4. In a few cases, no angular wall change was apparent and instead, the wall gradually thickened in the transition from common carotid to bulb. When this was observed, the operator positioned the measurement window on the most distal portion of the common carotid region not demonstrating the pre-bulb thickening. The longitudinal position of the analyzed segment for the replicate images of all subjects was carefully matched. To assist the operator to determine a 1 cm length of the wall, a movable graphics line scaled to 1 cm in the ultrasound imaging plane was superimposed on the display parallel to the lumen-intima echo.

3. Results

3.1. Phantom study results

A plot of the measured vs. true gap size for the step phantom is shown in Fig. 5a with subpixel interpolation enabled and in Fig. 5b with subpixel interpolation disabled. For gaps between 0.44 and 1.76 mm, the MAD between the gap size averaged over a 3 mm section of the wedge image using the computer tracking method and that measured with the optical comparator is 0.030 mm without subpixel interpolation and 0.020 with subpixel interpolation.

As described in Methods, the gap size was computed as the average of the 25 individual distance measurements obtained along the 3 mm length of each gap. To estimate the precision of individual distance measurements, we computed the standard deviation of the 25 distance measurements for each gap, with and without interpolation. The average standard deviation for 52 tracked gap images was 0.0235 mm without subpixel interpolation and 0.0092 mm with interpolation. These data appear to demonstrate that subpixel interpolation substantially improves the precision of the measurement.

The computer edge detection algorithm could not distinguish echoes closer than 0.33 mm and, as shown in Fig. 5a, gaps between 0.33 mm and 0.44 mm were overestimated. This overestimation results from the fact that the edge detection algorithm involves fitting a parabola over five pixels and when two edges are within four to five pixels of each other, the parabola fit to one edge is interfered with by the second edge. This problem can be partially solved by computing the gradient over fewer points, three for example, but then the edge detection becomes more noise-sensitive.

A better solution to the problem is to increase the image resolution, particularly in the direction perpendicular to the edges. Since the horizontal video resolution is higher than the vertical, ultrasound systems that rotate the image before generating the video output effectively increase pixel resolution between the edges. Analog image magnification, which is generally based on some form of pixel replication,

does not improve resolution but increasing ultrasound transducer frequency to 9–10 MHz can produce true resolution improvement.

For applications in which IMT serves as a clinical trial end point, absolute accuracy of the IMT measurement is not as important as the error in detecting IMT change. The absolute error in measuring the small gaps, as shown in Fig. 5a, is relatively high but the error in measuring the difference between two small gaps (roughly analogous to measuring a small change in IMT) is small. To show this error, we looked at the difference between the computer measurements of gap size for adjacent gaps minus the true gap size difference. If the true size of the nth gap on the horizontal axis of Fig. 5a is $T(n)$ and the corresponding computed gaps size shown on the vertical axis is $C(n)$, then for each n we calculated the change error as $e(n) = [C(n + 1) - C(n)] - [T(n + 1) - T(n)]$. A plot of $e(n)$ vs. $T(n)$ is shown in Fig. 6. The MAD of these errors is 0.012 mm, and the largest single error is 0.035 mm over a gap range of 0.33 mm to 1.76 mm.

3.2. Human replication study results, short-term variability

The MAD and the standard deviation S.D. average IMT from the replicate scans of 24 subjects were 0.033 mm and 0.041 mm, respectively, as shown in Table 1. The coefficient of variation (CV) for average IMT was 5.4%. The MAD and S.D. for maximum IMT were 3-fold and 2.5-fold greater, respectively, than for average IMT. The greater variability in maximum IMT results from calculating maximum IMT from a single edge pair compared with the determination of average IMT from approximately 84 edge pairs.

From the three scans of eight subjects by three sonographers, intersonographer CV and S.D. calculated from the first scan for each sonographer were found to be 3.9% and 0.026 mm, respectively. Intrasonographer CV and S.D. when calculated from replicate scans on the same day were 2.5% and 0.016 mm, respectively, and when calculated from the first and third scans obtained a week apart were 4.3% and 0.029 mm, respectively.

3.3. Human replication study results, long-term variability

The MAD and RMS errors in IMT measurement over 4 years from 143 scans of 12 MARS subjects were 0.021 and 0.030 mm, respectively. These data indicate the short- and long-term variability to be similar (Table 2).

4. Discussion

In clinical trials, the precision of the end point measurement determines the smallest change that can be detected. This in turn influences the length of a trial and the number of subjects that must be studied to achieve a specified significance level and power to detect change. Precision depends on the resolution and reproducibility of the measuring method. Manufacturers of ultrasound transducers frequently specify axial resolution as the minimum separation of two ultrasonically detectable objects. For the 7.5–9.0 MHz carotid transducers, axial resolution ranges from 0.2 to 0.4 mm. This definition of resolution, however, is useless for estimating the smallest change in separation that can be detected for two objects that are both more than the minimum distance apart to begin with.

In this study, we used a lucite phantom to show that with computer edge tracking incorporating subpixel interpolation, over a gap range from 0.44 to 1.76 mm, the average absolute error in measuring gap difference was 0.020 mm, with a maximum error of 0.035 mm. Clearly, the error in measuring IMT change in human carotid scans would be expected to be larger than the measured gap change in a lucite phantom, and the MAD of 0.041 mm obtained from the 24 replicate human scans confirms this. However, these data strongly support the idea that IMT changes can be detected that are 5–10 times smaller than the ultrasound axial resolution.

IMT measurement reproducibility has been assessed by several investigators with replication studies in humans. Reproducibility has been expressed variously by the MAD of paired measurements, by the S.D. of two or more replicate measurements or by the CV. A summary of these studies compared with the variability measurements using our automated edge tracking program is given in Table 2. With tracking method 1, as reported by Bond et al. [9], the operator measures maximum IMT by using a mouse to identify the lumen-intima and media-

adventitia at up to 10 discrete points spaced 1 mm apart on the displayed digitized image. Riley et al. [13] report on the variability of maximum IMT measurement using manual identification of 20 points spaced 0.5 mm apart, but their results cannot be directly compared because they report a combined 12 site average IMT that includes near and far walls of the common, bulb and internal carotid arteries of both the left and right side. With tracking method 2, reported in [3,5,7,8], the mouse is used to continuously trace the echoes from the digitized display and the computer is used to calculate average or maximum IMT from the hand-drawn boundaries.

As demonstrated in Table 2, variability of IMT measurement with our automated edge tracking method is 2–4 times lower than that obtained with manual tracking methods and appears equally precise over short periods (60 days) and long periods (48 months). The improvement in reproducibility of the automated method is most likely due to elimination of the variability associated with manual determination of edge coordinates and to the averaging of IMT at more than 80 points per cm. The computer edge finding is not only more reproducible than manual method but is also more accurate because of the sub-pixel interpolation used in the boundary location process.

The subjects in our studies demonstrated varying degrees of intima-media thickening but were generally free of advanced lesions in the distal CCA where the measurements were made. In the presence of advanced lesions, variability may be larger. Portions of irregular or raised lesion deflect the ultrasound signal away from the transducer, producing gaps in the wall echo. Calcified lesions prevent the transmission of the ultrasound signal through the lesion and thus prevent imaging of the wall 'behind' the lesion. In addition, very small changes in transducer position can substantially change the image of complex lesions. Since comparative studies in Table 2 may have included subjects with advanced lesions, a portion of the variability difference between the manual and automated methods may be accounted for by differences in the study populations. Further studies of comparable subject populations are required before the various methods can be precisely compared.

At present, the automated tracking procedure has only been tested in the far wall of the common carotid and, as we have demonstrated in two randomized lipid-lowering clinical trials, it has proved to be excellent for measurement of small IMT changes in arteries without advanced lesions. Variability of the automated IMT method for the near wall was not determined in this study because of questions suggested by others about the reliability of near wall IMT measurements [14]. The variability of automated IMT measurement in the bifurcation and internal carotid regions is likely to be higher than that in the CCA because of the image gaps and transducer positioning problems associated with complex lesions, as discussed above. These are of course also problems for manual tracking methods. Since the association of risk factors, hemodynamic factors and extent of lesion formation in the bifurcation and internal carotid are likely different from those in the common carotid region, it is important that the automated method be studied in these regions.

The current automated IMT method deals with the intermittent echoes from complex lesions by testing the strength of the detected edges and then calculating IMT as the average thickness of those portions of the lesion boundary that are well defined. This procedure is valid only if the well-defined portions of the boundary form a representative sample of the entire boundary. Another way to deal with these lesions is to track the well-defined portions of the lesions with the automated procedures and then use an interpolating procedure to fill in the gaps. This procedure only approximates IMT but has an advantage over manual tracking methods of minimizing variability on the portions of the lesion that can be tracked. The combined tracking/interpolation procedure has not yet been implemented. However, as a practical matter, the PROSOUND IMT measurement program allows manual tracking to be substituted for automated tracking for very complex lesions. No manual tracking was used in the studies described in this paper.

Based on the S.D. of 0.04 mm for measurement of average IMT obtained with this method of image analysis in the short-term reproducibility study, it is estimated that a two-arm trial of 28 subjects per group could detect a treatment difference in IMT of 0.03 mm with 80% power. By comparison, for

the IMT S.D. value given in Table 2 of 0.08 mm [3], 112 subjects per group would be required in order to detect 0.03 mm treatment differences with the same power and for an S.D. of 0.011 mm [8], 295 subjects per group would be required. In CLAS, a significant treatment difference of 0.09 mm in IMT change was demonstrated between 24 colestipol/niacin treated subjects and 22 placebo treated subjects after 2 years of intervention ($P < 0.0001$) and 0.12 mm after 4 years ($P < 0.0001$) [15]. Additionally, after 1 year's intervention in 26 CLAS subjects, an IMT difference of 0.03 mm was detected between treatment groups ($P < 0.01$) [16]. In the MARS, an independent study using a different lipid lowering agent (lovastatin) but utilizing the same ultrasound methodology, CLAS results were corroborated. Analyzing the ultrasound data for CLAS-like men in MARS, i.e. non-smoking males with coronary artery bypass grafts, a significant treatment difference in 2 year IMT change between 15 lovastatin treated subjects and 15 placebo treated subjects of 0.13 mm was demonstrated ($P < 0.0006$) [17].

5. Conclusions

Since Pignoli et al.'s 1986 description and pathological corroboration that B-mode ultrasound could measure IMT [1], there has been a steady increase in refinement of ultrasound imagery. High resolution two-dimensional ultrasonography at present is capable of delivering superb quality images with axial resolution between 0.2 and 0.4 mm. Although B-mode ultrasound measurements of IMT have rapidly become assessment tools in clinical trials and large cardiovascular epidemiologic studies, variability of IMT measurements from these high quality images has remained high relative to the small incremental changes in IMT. The automated edge detection method presented in this paper represents a major advance for measurement of average IMT in the CCA from B-mode ultrasound images, with variability substantially reduced (two to four times) compared with prior methods.

Acknowledgments

This study was upported in part by the National Heart Lung and Blood Institute grants HL-40098, HL-23619, HL-45005 and HL 49885, with additional support from Upsher-Smith, Upjohn and Merck Sharpe and Dohme.

References

[1] Pignoli, P., Tremoli, E. and Poli, A., Intimal plus medial thickness of the arterial wall: a direct measurement with ultrasound imaging, Circulation, 74 (1986) 1399.

[2] Salonen, R., Haapanen, A. and Salonen, J.T., Measurement of intima-media thickness of common carotid arteries with high resolution b-mode ultrasonography: inter- and intra-observer variability, Ultrasound Med. Biol., 17 (1991) 225.

[3] Persson, J., Stavenow, L., Wikstrand, J., Israelsson, B., Formgren, J. and Berglund, G., Noninvasive quantification of atherosclerotic lesions. Reproducibility of ultrasonographic measurement of arterial wall thickness and plaque size, Arteriosclerosis Thromb., 12 (1992) 261.

[4] Beach, K.W., Isaac, C.A., Phillips, D.J. and Strandness, D.E., An ultrasonic measurement of superficial femoral artery wall thickness, Ultrasound Med. Biol., 15 (1989) 723.

[5] Salonen, J.T. and Salonen, R., Ultrasonographically assessed carotid morphology and the risk of coronary heart disease, Arteriosclerosis Thromb. 11 (1991) 1245.

[6] Heiss, G., Sharrett, A.R., Barnes, R., Chambless, L.E., Szklo, M. and Alzola, C., Carotid atherosclerosis measured by B-mode ultrasound in populations: associations with cardiovascular risk factors in the ARIC study, Am. J. Epidemiol., 134 (1991) 250.

[7] O'Leary, D.H., Polak, J.F., Wolfson, S.K. et al., Use of sonography to evaluate carotid atherosclerosis in the elderly: the cardiovascular health study, Stroke, 22 (1991) 1155.

[8] Wendelhag, I., Wiklund, O. and Wikstrand, J., Arterial wall thickness in familial hypercholesterolemia. Ultrasound measurement of intima-media thickness in the common carotid artery, Arteriosclerosis Thromb., 12 (1992) 70.

[9] Bond, M.G., Barnes, R.W., Riley, W.A. et al., High-resolution B-mode ultrasound scanning methods in the Atherosclerosis Risk in Communities study (ARIC), J. Neuroimaging, 1 (1991) 68.

[10] Poli, A., Tremoli, E., Colombo, A. et al., Ultrasonographic measurement of the common carotid artery wall thickness in hypercholesterolemic patients, Atherosclerosis, 70 (1988) 253.

[11] Bonithon-Kopp, C., Scarabin, P., Taquet, P. et al., Risk factors for early carotid atherosclerosis in middle-aged French women, Arteriosclerosis Thromb., 11 (1991) 966.

[12] Cashin-Hemphill, L., Kramsch, D.M., Azen, S.P. et al., The monitored atherosclerosis regression study (MARS): design, methods and baseline results, Current Clinical Trials (serial online), Document 26, 23 October 1992.

[13] Riley, W.R., Barnes, R.W., Applegate, W.B. et al., Reproducibility of noninvasive ultrasound measurement

Note to editor

There are no changes to remaining pages.

of carotid atherosclerosis: the Asymptomatic Carotid Artery Plaque study, Stroke, 23 (1992) 1062.
[14] Wendelhag, I., Gustavsson, T., Suurkula, M. et al., Ultrasound measurement of wall thickness in the carotid artery: fundamental principles and description of a computerized analysing system, Clin. Physiol., 11 (1991) 565.
[15] Blankenhorn, D.H., Selzer, R.H., Crawford, D.W. et al., Beneficial effects of colestipol–niacin therapy on carotid atherosclerosis: two and four year reduction of intima media thickness measured by ultrasound, Circulation, 38 (1993) 28.
[16] Mack, W.J., Selzer, R.H., Hodis, H.N. et al., One-year reduction and longitudinal analysis of carotid intima-media thickness associated with colestipol/niacin therapy, Stroke, 24 (1993) 1774.
[17] Mack, W.J., Hodis, H.N., Pogoda, J.M. et al., Reduction of carotid artery intima-media thickness with lipid lowering therapies. A comparison of two clinical trials, J. Am. Coll. Cardiol., 21 (1993) 166A.

Table 1
Results of the short-term human common carotid replication study (24 subjects)

	Average IMT (mm)	Maximum IMT (mm)
Pooled mean value	0.740	0.979
MAD	0.033	0.099
S.D.	0.041	0.109

Table 2
IMT measurement variability studies of the distal common carotid artery far wall

Reference	Mean IMT		Maximum IMT		N[a]	Tracking method[b]
	MAD (mm)	S.D. (mm)	MAD (mm)	S.D. (mm)		
9				0.11[c]	1422	1
8		0.11[d]		0.13[d]	50	2
3		0.08			65	2
2				0.087	60	2
7	0.13		0.14		122	2
Present study						
Short term	0.033	0.041	0.099	0.109	48	3
Long term	0.021[e]	0.030[e]			143	3

[a] N, number of scans, including replications.
[b] Tracking methods: (1) manual selection of 10 discrete points with a mouse; (2) manual continuous tracing with a mouse; (3) automatic edge finding.
[c] Anterior view.
[d] Computed from coefficients of variation.
[e] MAD was calculated as the mean absolute difference between the IMT values measured over time and a linear regression line fit to the values. S.D. was calculated as the RMS difference of the measured values and the regression line.

Fig. 1. Example of image intensity values and computed gradient at one point of the lumen-intima echo.

Fig. 2. Lucite phantom used to measure resolution.

Fig. 3. IMT values for two subjects in the MARS study measured over a 4 year period. The linear regression line is also shown.

Fig. 4. B-mode distal common carotid image showing proximal portion of the bulb region used as reference for positioning the edge tracking window. Portions of the wall where acceptable edge pairs were located are also shown.

Fig. 5. (a) Measured vs. true gap size for step phantom using sub-pixel interpolation to locate echoes reflected from the gaps in the lucite. (b) Same measurement as shown in (a), without sub-pixel interpolation.

Fig. 6. Estimated error in measuring change in gap size from the step phantom.

Fig. 1. ATH 5305 80%

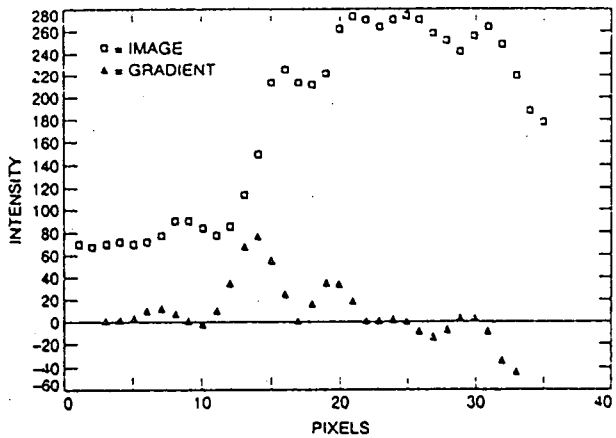

Fig. 2. ATH 5305 80%

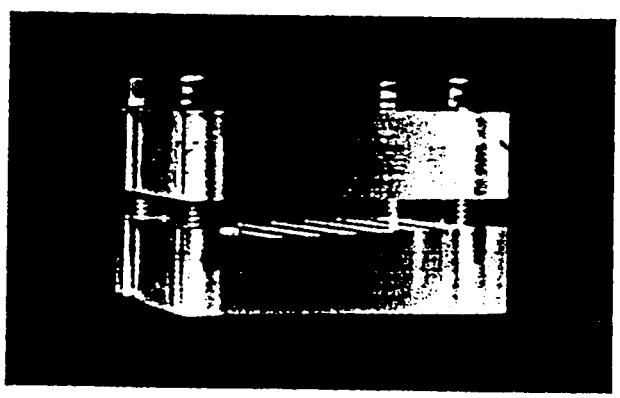

TRIM | | TRIM

Figs 3(A+B) ATH5305 758

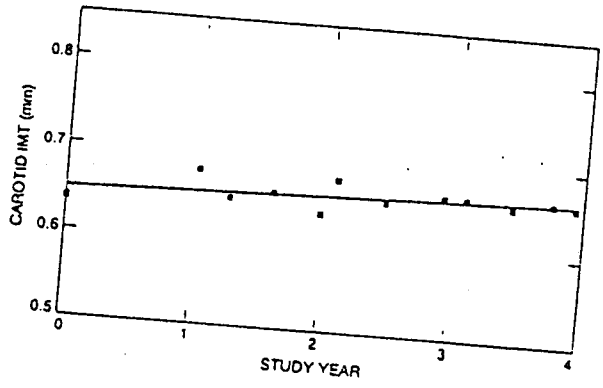

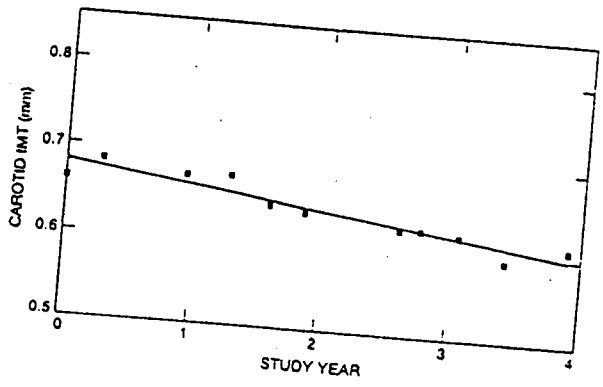

Fig. 4. ATH5305 606

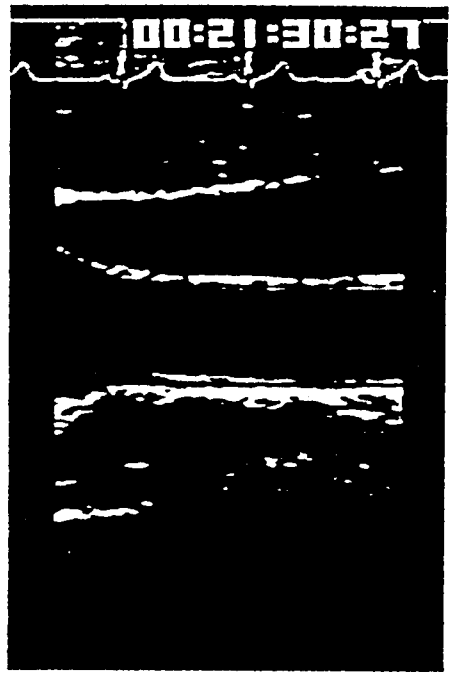

Figs 5(A+B) ATH5305

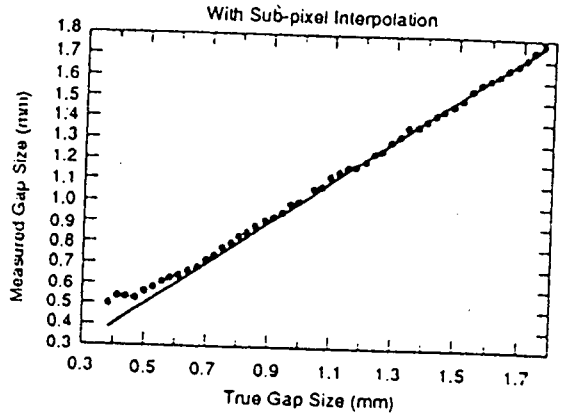

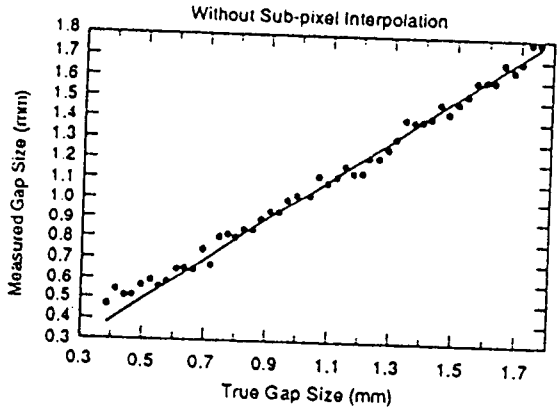

Fig. 6. ATH5305 95%